Design principles for interface reaction in all-solid-state batteries

Xin Li*

In the past decade, with the development of solid-state batteries, many promising results have emerged in the field, suggesting that it can be a paradigm-shift solution to next-generation mobile energy storage with the potential for breakthrough performance beyond commercial Li-ion batteries. This article attempts to explain the unique fundamental mechanism that dominates interface reaction in a solid-state battery. The interface reactions that largely limited the battery performance in the early stage of the field instead become the design opportunity to unlock many breakthrough performances. This article will focus on explaining the fundamental principles regarding how electrochemical interface reactions are locally coupled with mechanical and transport properties to dictate battery performance, particularly through dynamic voltage stability, giving opportunities to design electrolyte and interface coating materials for advanced battery performance.

Introduction

An early motivation for using solid electrolytes to replace liquid electrolytes is the possibility to increase the safety of batteries. Not only is the solid electrolyte less flammable, but there is also a hope that the mechanical strength of the solid ceramic electrolyte could block the lithium dendrite penetration to prevent a short-circuit of batteries. A sufficiently dense ceramic electrolyte separator layer is thus naturally wanted. However, the dendrite growth process could be robust enough driven by battery cycling to find all of the possible existing pathways and even create new cracks to penetrate.[1,2] Thus, engineering a sufficiently dense ceramic electrolyte layer to prevent dendrite has been a big challenge.

Unlike the mechanically stiff oxide electrolyte, it is less challenging for the soft sulfide and halide electrolytes to form a relatively dense layer by the cold press calendering process that is widely used in the battery industry, due to the low bulk, shear, and yield moduli.[3–7] After the cold press of a sulfide electrolyte layer, there can still be 5 to 15 percentages of remaining porosity. Whether such a separator electrolyte layer can prevent the dendrite penetration depends on other aspects of the battery design, at both device and material levels.

External pressure during battery operation is an important device-level parameter. Although from a practical device perspective the external operational pressure must be reduced to a low level, initial performance demonstrations of sulfide and halide solid-electrolyte-based batteries were mostly under high operational pressure using a simple pressurized coin cell.[8–10] This is because it is the simplest way to ensure good interface contact between dry powder so that scientists can have an electrochemically functional solid–solid interface to develop and test electrolyte and electrode materials. Meanwhile, people are also forced to directly face the new challenges arising from such an interface, which is electrochemically quite different from the conventional solid–liquid interface.

Importantly, these closely contacted solid–solid interfaces form the mechanical constriction[11–13] to any local volume expansion from decompositions induced by interface chemical and electrochemical reactions, which is a unique effect in all-solid-state batteries in comparison with batteries with liquid inside, causing different reaction pathways thermodynamically and kinetically. This is because now reaction Gibbs energy, G, is strongly coupled with various variables and thus is a function of them, which include local strain, stress, and any induced diffusion and reaction limiting processes.

For these all-solid-state batteries, to be compatible with a future industrial scale-up, one goal of material and device development is to demonstrate performance metrics at low operational pressure of a few megapascals or below, while simultaneously aiming to maintain the performance that was

Xin Li, John A. Paulson School of Engineering and Applied Sciences, Harvard University, Cambridge, USA; lixin@seas.harvard.edu

doi:10.1557/s43577-023-00626-0

previously demonstrated at high operational pressure. Without understanding the real function of external pressure and taking the right approach to compensate for it, directly lowering the pressure, however, often significantly lowers the initial capacity or critical current density and quickly decays the cycling capacity. Therefore, it is of particular interest to obtain a fundamental understanding about how to make those previous innovations transferable to the lower pressure regime upon a proper battery design.

For example, because one role of the operational pressure is to maintain a low porosity and good interface contact during battery cycling, it is thus important to develop advanced battery formation and assembly procedures to maintain the same level of contact at a low pressure, such as introducing the right polymer binders[14] and more deformative electrolyte materials.[15] Also, if we assume at low pressure the effective area of a well-connected interface is reduced, then developing a faster Li-ion conductor[16] will be of more importance, in addition to the obvious capacity benefit at low temperature. Furthermore, because interface electrochemical reactions are modulated by the mechanical constriction condition, represented by the mechanical constriction modulus K_{eff}, rather than the external pressure, many materials chemistry and battery configuration innovations[17–20] made to stabilize such interfaces, initially tested in batteries at high external pressure, can thus be transferable to low operational pressure, if additional methods can be introduced to maintain a close interface contact during the battery operation.

Importantly, controlling the evolution of an interface reaction, rather than completely preventing them from happening, has become a useful design principle to advance the battery performance. Such interface reactions can be used to arrest lithium dendrite growth through self-limited localized decomposition of a solid electrolyte[19] and is also inherent behind the expanded operational voltage window beyond the thermodynamic voltage stability limit of the electrolyte to work with high-voltage cathode materials.[12,21] Furthermore, when reaching the external pressure regime of 10 MPa or below, pores can also form in the plated or stripped lithium metal layer, especially at a high current density.[22] This further emphasizes the importance of designing beneficial dynamics of anode interface reactions for dendrite suppression, through material and device innovations, which could include the thin graphite protection layer[20] that covers the lithium-metal anode, the Si, Si-C, Mg alloys, and Ag-C anodes[14,23,24] that assist more homogeneous lithium plating,[24] and the multi-electrolyte-layer configuration that suppresses Li dendrite penetration.[19]

It is worth noting that a recent work shows that under an external pressure of 7 MPa or above, the lithium plating can be easier to generate cracks than under 0.1 MPa pressure,[25] pointing out a potential performance benefit by lowering the operational pressure. Furthermore, at a lower pressure of 2–3 MPa, the sulfide electrolyte-based solid-state battery was also demonstrated with 30 mg/cm^2 cathode loading at 0.5 C for 1000 cycles.[14] These results suggest the opportunity for low-pressure solid-state batteries not only to maintain, but also surpass, the battery performance at a high pressure, upon overcoming those remaining technical barriers.

This article focuses on the fundamental understanding of interface reactions under mechanical constriction that is behind many important experimental innovations in solid-state batteries. Although the initial experiments reported in the field that inspired the physical picture and the constrained ensemble description of such interface reactions were mostly performed at a high operational pressure, the knowledge is in fact transferable to the design of low-pressure solid-state batteries, because a global external operational pressure is not a fundamental variable in the constrained ensemble description.

Under the local mechanical constriction, it is the coupling of local reaction strain (ϵ), stress (σ), and effective stress (σ_{eff}) with Gibbs reaction energy $G(\epsilon, \sigma, \sigma_{\text{eff}})$ that dictates the interface reaction through a unique dynamic voltage stability, which contains both thermodynamic metastability and kinetic stability. One essential aspect of the dynamic voltage stability here, counterintuitively, is to design and utilize the initial interface instability. The effect can be utilized to innovate new materials and devices in combination with other approaches to design advanced low-pressure solid-state batteries with higher cycling stability against interface degradation at high current densities, with the potential to break the technical limit set by commercial Li-ion batteries.

Self-limiting decomposition reaction at solid–solid interface

The standard convex-hull computational approach has been useful to calculate the voltage stability window for liquid-electrolyte Li–ion batteries, which is also the method to precisely calculate the intrinsic thermodynamic voltage window of solid electrolytes.[26,27] Above this voltage window, the oxidization decomposition reaction will occur, while below it, the reduction reaction will occur. The self-decomposition of a liquid electrolyte and the interface decomposition, in principle, can both be calculated by the approach[18] (**Figure 1**a), where the yellow star in the illustration refers to the liquid-electrolyte phase (when calculating the electrolyte self-decomposition) or the pseudo-phase (when calculating the interface reaction between liquid electrolyte and solid electrode). Because there is a hull energy of $G_{\text{hull}} > 0$ for the reaction at a given lithium chemical potential or electrochemical voltage, the phase or pseudo-phase above the hull will decompose to D_1 and D_2 phases that are on the "convex hull" in the illustration.

If a liquid electrolyte is added to the solid-state battery (i.e., it is not an all-solid-state battery anymore), the predicted voltage window from the standard convex hull approach in many cases can match well with the experiment. For example, the narrow intrinsic voltage window of a sulfide solid electrolyte from 1.7 to 2.3 V is such a case,[12] beyond which sulfide solid electrolytes were found to deeply decompose. Note that the liquid electrolyte cannot provide a mechanical constriction

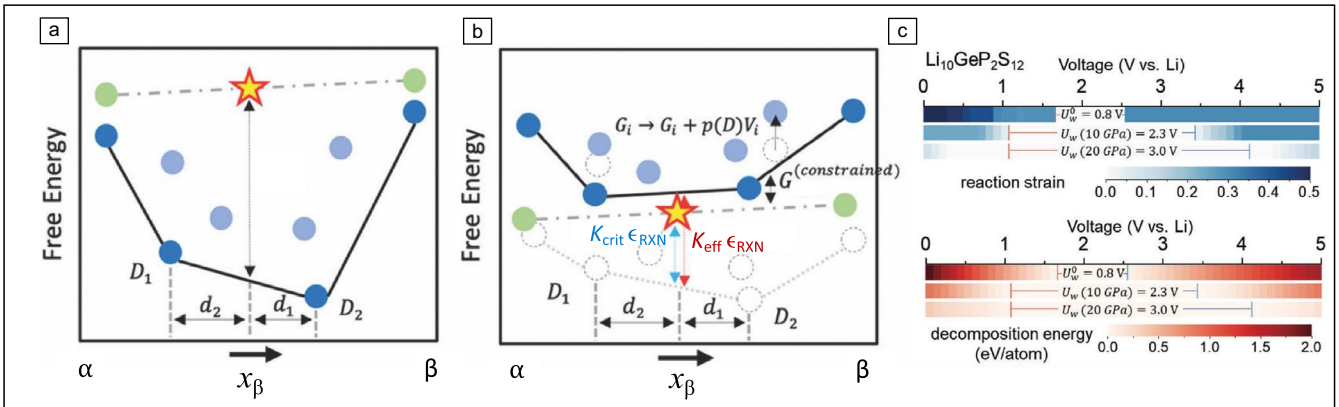

Figure 1. (a) Convex hull illustration for pseudo-phase models of the solid interface reaction. The yellow star represents the interphase composition (*x*-axis) and energy (*y*-axis) of the two reactive phases represented by green dots. The dark blue dots represent phases that are thermodynamically favorable, and the black line represents a linear combination of these phases (i.e., the convex hull).[18] (b) An illustration about how mechanical constriction modulus K_{eff} impacts the interphase convex hull. When $K_{eff} > K_{crit}$, the interphase is now lower in free energy than the decomposition products on the hull due to $K_{eff}\epsilon V$.[18] (c) Electrolyte dynamic voltage stability window, reaction strain, and decomposition energy in response to constriction by direct minimization method using LGPS as an example.[28] (a–b) Reprinted with permission from Reference 18. © 2021 Royal Society of Chemistry. (c) Reprinted with permission from Reference 26. © 2023 Wiley.

so in principle K_{eff}=0 GPa. Another example without liquid being involved is to put lithium metal in direct contact with sulfide electrolyte, such as $Li_{10}GeP_2S_{12}$ (LGPS), where the interface chemical decomposition can happen immediately during the battery assembly[19] that is thus a process initially under little mechanical constriction at time $t = 0$ ($K_{eff}^{t=0} = 0$). These decomposition reactions give $Li_{15}Ge_4$ alloy and Li_3P in experiment following **Equation** 1, where both Ge and P are in highly reduced valence states, consistent with the standard convex hull prediction.

$$LGPS + 23.75Li \xrightarrow{K_{eff} = 0\ GPa} 0.25Li_{15}Ge_4 + 2Li_3P + 12Li_2S \quad (1)$$

$$LGPS + 14Li \xrightarrow{K_{eff} > 10\ GPa} GeP_2 + 12Li_2S \quad (2)$$

In an all-solid-state battery without any liquid electrolytes, however, it was found that to describe the full evolution process of interface reactions, a modification of the standard convex hull approach is needed in order to make a more relevant comparison with experiments in many cases. First, going beyond the intrinsic voltage stability window, only a limited level of decomposition of a solid electrolyte was observed rather than the deep or even complete decomposition when a liquid electrolyte is added. Further decomposition can be well inhibited at such a mechanically constricted solid–solid interface, thus still giving a functional battery performance.

That means sulfide solid electrolytes can show a much wider operational voltage window[12,21] in practical solid-state batteries than the standard convex-hull computational prediction. This experimental fact forms the foundation that sulfide electrolyte-based solid-state batteries can cycle with a 4 V cathode and 0 V lithium-metal anode.[14,19,23] In the previous example of the solid–solid interface of Li|LGPS, further decomposition is inhibited, as the local mechanical constriction after the initial decomposition evolves to nonzero values at time $t_1 > 0$ (i.e., $K_{eff}^{t_1 > 0} > 0$). The LGPS phase can still be well observed from x-ray diffraction (XRD), although the thick decomposition interphase makes the primary interface electrochemically dead without sufficient ionic conductivity when the Li metal layer is in direct contact with the LGPS layer.

Furthermore, when the electrolyte is separated from direct contact with the Li metal in the battery assembly by a thin graphite layer,[20] to avoid the initial primary interface contact at $K_{eff}^{t=0} = 0$, it is found that lithium metal will be mixed with graphite to form a composite layer during battery cycling, so local interface contact points are formed *in situ* with more interface reactions at $K_{eff}^{t_1 > 0} > 0$. Now it can be more easily observed from experiments that the decomposition pathway is changed, where GeP_2 becomes the product instead, which is a phase with much less-reduced valence states for Ge and P. This means under mechanical constriction, the reduction level of the decomposition at anode (or oxidation if at cathode) can be suppressed by mechanical constriction. We find that at a local effective constriction modulus K_{eff} above 10 GPa and effective constriction stress σ_{eff} around 3 GPa[12,21] (since $\sigma_{eff} = \epsilon K_{eff}$), the predicted decomposition reaction based on our constrained ensemble computational platform follows **Equation** 2 that gives GeP_2 as the product, agreeing well with experiment. Note that the actual local stress σ can be much smaller than 3 GPa, as the effective stress σ_{eff} also contains the effective contribution from kinetic effects (i.e., σ_k), to be discussed later (i.e., $\sigma_{eff} = \sigma + \sigma_k$).

If we borrow the framework of the convex-hull computational approach, the experimental fact of a wider operational voltage window means that the phase (solid electrolyte) or pseudo-phase (interface between the solid electrolyte and electrode materials) that was above the hull in the energy-composition space at the beginning of the decomposition when

$K_{\text{eff}}^{t=0} = 0$ (the yellow star in Figure 1a) should have the ability to quickly evolve to zero or negative hull energy (G_{hull}) to avoid further decomposition when $K_{\text{eff}}^{t_1>0} > 0$[18] (the yellow star in Figure 1b). This evolution is thus a dynamic process, which also indicates that a modified convex hull approach that considers the K_{eff} driving force for the evolution is needed to describe such a unique "dynamic voltage stability," or simply, "dynamic stability" at the solid–solid interface under mechanical constriction. Due to this effect, the decomposition products are also changed away from D_1 and D_2 at zero constriction to other products at nonzero constriction, which is also the principle underlying the specific case of changing from $Li_{15}Ge_4$ and Li_3P at $K_{\text{eff}}=0$ GPa to GeP_2 at $K_{\text{eff}}=10$ GPa as previously discussed (Equations 1 and 2). The simplest explanation is that higher K_{eff} will select reactions with smaller reaction strain and energy to happen (Figure 1c), as systematically demonstrated in a recent work.[28] The effect causes a greatly expanded voltage window (Figure 1c).

The dynamic stability and the nonzero effective modulus $K_{\text{eff}}^{t_1>0}$ are originated from the decomposition reaction itself, which suggests that it is a self-limiting decomposition. These interface reactions are often with positive reaction strains (i.e., $\epsilon > 0$), meaning that the reaction products are larger in volume than the reactants.[29] Note that in calculating the volume change, the Li metal volume is not counted as reactant (i.e., in a reduction reaction), but it is counted as product (i.e., in an oxidization reaction). For example, in the reduction reaction of Equations 1 and 2, the volume of Li metal on the left side is not counted. This is because it is the volume change of the solid-electrolyte side in the interface reaction that is relevant to the effects of particular interest here. More specifically, Li was absorbed into the electrolyte through the decomposition reaction with volume expansion into the local sites of solid electrolyte. In contrast, in an oxidative reaction, the Li metal reaction product is encapsulated within the decomposition composite, contributing to the local positive reaction strain. In both reduction and oxidation reactions, reaction products are encapsulated by the reaction front that is ionically passivated (will discuss later), thus no Li ions can escape from the ionically screened decomposition region. The Li^+ ions and electrons that must leave the cathode or anode to complete such electrochemical reactions are from the ion and electron reservoir outside the local decomposition region defined by the reaction front.

If the reaction continues without a stop, the inhomogeneous local volume expansion will for sure detach the interface between particles or even create cracks inside the electrolyte particles, regardless of external pressure, because the 1–100 MPa scale of the external pressure is 10–1000 times smaller than the scale of any reaction-induced local stress. However, it was found that in a properly designed solid-state battery even under low or moderate external pressure (1–25 MPa), reaction-induced loose contacts and cracks can be largely avoided, and the reaction can be limited at a very early stage.

For example, in the multi-electrolyte-layer configuration (**Figure 2**a), the central electrolyte layer that is reactive with Li based on the standard convex hull prediction can instead serve to prevent the lithium dendrite penetration using dynamic stability, where the dendrite growth is arrested by the reaction to prevent the penetration, thus little cracks were observed after long cycling at high current densities. Although the initial demonstration of the multi-electrolyte-layer design was performed at high operational pressures of 100–250 MPa and a low cathode loading of 2 mg/cm^2 in a pressurized cell,[17,19] more recently, the pressure has been reduced to 5–25 MPa for a slurry-casted pouch cell, where 5000+ cycles have been demonstrated at a high cathode loading above 15 mg/cm^2 at a high C-rate of 5 C charge and 5 C discharge.[24] Furthermore, at lower pressures of 2–3 MPa the argyrodite Li_6PS_5Cl (LPSCl1.0) sulfide electrolyte-based solid-state battery was also demonstrated with 30 mg/cm^2 cathode loading at 0.5 C for 1000 cycles, where the lithium plating is assisted by a Ag-C composite layer in direct contact with LPSCl1.0.[14]

These experiments also suggest that it is not the external pressure in the megapascal regime that makes the reaction self-limiting. Instead, it more reflects a certain intrinsic property of such a solid–solid interface under mechanical constriction utilized by a proper battery design. In fact, to reduce the hull energy (G_{hull}) to zero, the effect of interest here needs to interact with the positive reaction strain (ϵ) by gigapascal level of effective constriction modulus (K_{eff}), so that $G_{\text{hull}} = K_{\text{eff}}\epsilon V$,[17,18] where V is the reference volume (Figure 1b). The effective constriction modulus K_{eff} often needs to be at the level of 5–15 GPa for sulfide and halide solid electrolytes to suppress the decomposition, and the "effective constriction stress" σ_{eff} is calculated by multiplying K_{eff} with ϵ. Because the reaction strain ϵ is often around 30% at low K_{eff} and further decreases to approach zero with increasing K_{eff} (as

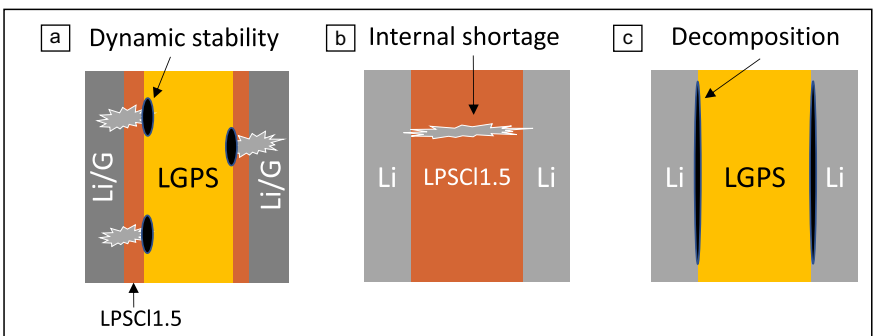

Figure 2. (a) Multi-electrolyte-layer design in a symmetric battery configuration of Li|graphite (G)|$Li_{5.5}PS_{4.5}Cl_{1.5}$(LPSCl1.5)|$Li_{10}GeP_2S_{12}$(LGPS)|LPSCl1.5|G|Li with dynamic voltage stability to prevent Li dendrite penetration. (b) Symmetric battery of Li|LPSCl1.5|Li with dendrite penetration-induced short circuit. (c) Symmetric battery of Li|LGPS|Li with severe primary interface decomposition-induced diffusion impedance.

higher K_{eff} energetically prefers reactions with lower reaction strain, as illustrated in Figure 1c), the σ_{eff} is usually less than 4 GPa here.

Because the magnitudes of σ_{eff} and the fracture stress limit σ_{frac} of these electrolyte materials are comparable, the fact that in many cases the decomposition is inhibited at an early stage without crack formation suggests that the effective terms of stress σ_{eff} and modulus K_{eff} include a significant contribution with an effective kinetic origin (i.e., σ_k), so that the actual local stress σ is less than the fracture stress limit σ_{frac} (i.e., $\sigma < \sigma_{frac}$), even if $\sigma_{frac} < \sigma_{eff}$, where $\sigma_{eff} = \sigma + \sigma_k$.

Diffusion limit at reaction front and critical role of inhomogeneous lithium chemical potential

In a liquid-electrolyte environment, the electrolyte decomposition reaction can sufficiently develop due to thermodynamic instability with the electrode, because the local chemical potential of Li^+ ion is homogeneously surrounding the interface. In an all-solid-environment, however, the local chemical potential is not homogeneous anymore, as numerous point contacts at (sub)nanoscale are inevitable, even the solid–solid interface was pressed to form a close contact at micrometer scale (**Figure 3**a). The local reaction strain field at these point contacts are thus inhomogeneous with a large local curvature (Figure 3b), unlike the flat reaction front in a homogeneous liquid environment.

Experimentally, it was found that the LGPS phase can completely decompose if being charged to 3.2 V in a liquid environment, while the phase is almost intact in XRD except for some strain broadening[12,19] analyzed from the slightly increased width of XRD peaks. A similar phenomenon was also found for argyrodite sulfide electrolytes. This suggests that a flat reaction front at liquid–solid interface is much easier to propagate the decomposition deeply than a reaction front with large local curvature at the solid–solid interface. This is because the former can more easily release the local strain field to the environment, giving less steep variance of local strain at reaction front and thus a much smaller and ineffective σ_k, while the latter will hold the coupling of the tensile ($\epsilon > 0$) and compressive ($\epsilon < 0$) plastic strain fields on the two sides of the curved reaction front at nanoscale with a much larger σ_k that well divides the regions of decomposition product and the undecomposed electrolyte (Figure 3c).

The strain field near the reaction front is the origin of both the XRD strain broadening and the self-limiting decomposition that maintains the crystalline phase of the electrolyte materials charged beyond the intrinsic voltage stability window. The strain field induced by reaction has also been observed by x-ray absorption spectroscopy in other sulfide electrolytes,[12,30] unveiling the PS_4 tetrahedron deformation.

The atomic-scale lattice compression at one side of the reaction front with $\epsilon < 0$ is critical to limit further decomposition by the ionic passivation. It was found that a 5–10% of local compressive strain to the crystalline lattice[12,24] at the reaction front can already dramatically decrease the diffusivity of ions by orders of magnitude (i.e., diffusivity $D \to 0$ in Figure 3c). This diffusion-limiting process leads to an ionic passivation at the surface that encapsulates the decomposed region to prevent further propagation of reactions, as any decomposition will need certain ionic interdiffusion to happen kinetically.[12]

Interface reactions will thus feel a significant effect from an additional energy stabilization term, $E_{kinetic}$, derived from such kinetic stability effect, giving a much wider interface voltage stability than what can be provided by thermodynamic intrinsic stability and the metastability. The thermodynamic metastability to suppress the interface voltage reaction is from the strain energy E_{strain} that integrates the curve of actual local stress and strain (i.e., $E_{strain} = \int \sigma V d\epsilon$). However, the magnitude of the strain energy is limited by the plastic deformation and the fracture limit of electrolyte materials, beyond which there is no local mechanical constriction. Because both energy terms of E_{strain} and $E_{kinetic}$ share the same local reaction strain term ϵ, we have $E_{kinetic} = \int \sigma_k V d\epsilon$, which defines the kinetic part of the effective stress σ_k. The total stabilization energy that

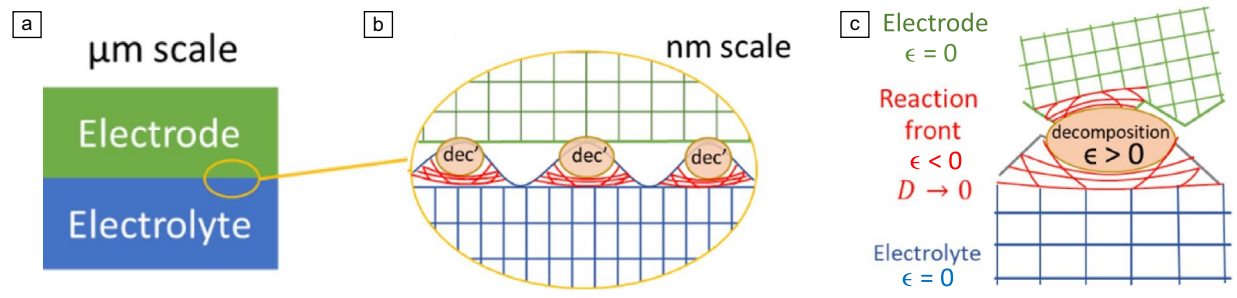

Figure 3. (a) Illustration of close interface contact at micrometer scale between electrode and electrolyte particles. (b) Inhomogeneous contact at a solid–solid interface with (sub)nanometer point contacts and gaps, giving spatially inhomogeneous decompositions. (c) Reaction front at a point contact, where tensile strain ($\epsilon > 0$) of the decomposition reaction induces compressive plastic strain field ($\epsilon < 0$) in the undecomposed electrolyte region that immediately wraps the reaction front (red region), causing a significant drop of ionic diffusivity ($D \to 0$) and the ionic passivation to further decomposition. More details can be found in a recent work.[28] Reprinted with permission from Reference 28. © 2023 Wiley.

includes both thermodynamic metastability and kinetic stability for interface reactions beyond the thermodynamic intrinsic stability is thus $E_{total} = E_{strain} + E_{kinetic} = \int(\sigma + \sigma_k)Vd\epsilon$, which also defines the total effective stress $\sigma_{eff} = \sigma + \sigma_k$.

Because $\sigma_{eff} = \epsilon K_{eff}$, we also have the effective mechanical constriction energy $E_{total} = \epsilon K_{eff} V$ in the simplest form, obtained from the linear term in a Taylor expansion if assuming local infinitesimal reaction enters the plastic region quickly, which is also a useful approximation for the high-throughput computational search and design of interface reactions. However, as previously discussed, the mechanical constriction modulus K_{eff} evolves with time in the dynamic process of the interface reaction (e.g., Figure 1 and Equations 1 and 2). Fundamentally, this is because the reaction strain field evolves with time (i.e., $\epsilon(x,t)$), thus more precisely, both effective terms depend on $\epsilon(x,t)$, i.e., $\sigma_{eff}(\epsilon(x,t))$ and $K_{eff}(\epsilon(x,t))$, giving $E_{total} = \int \sigma_{eff}(\epsilon(x,t))Vd\epsilon(x,t) = \int \epsilon^n(x,t)K_{eff}(\epsilon(x,t))Vd\epsilon(x,t)$. Thus, a more precise treatment of these details may deviate E_{total} away from the linear dependence of ϵ.

This effect gives the kinetic effective stress σ_k beyond the actual local stress σ, forming one critical component of the dynamic voltage stability. The ionic passivation gives the self-limiting nature of the decomposition that was observed at the interface between lithium dendrite and electrolyte[19] (e.g., Figure 2a), and cathode–electrolyte interface as well.[28]

Materials dependence of dynamic voltage stability and electrochemical stability

There is an obvious material dependence in interface electrochemical stability and dynamic stability, which gives the opportunity to search and design advanced materials for solid-state battery applications. Sulfide electrolyte materials not only show very different electrochemical voltage stabilities in solid-state batteries, but they also show different dynamic voltage stabilities. For example, $Li_{5.5}PS_{4.5}Cl_{1.5}$ (LPSCl1.5) is more stable in direct contact with lithium metal (Figure 2b), whereas LGPS is less stable with lithium metal (Figure 2c). Thus, the decomposition at the primary interphase between LGPS and Li metal, although being self-limited, can still develop sufficient thickness and ionic impedance. In contrast, the primary interface between LPSCl1.5 and Li metal shows much less decomposition, but short circuit by Li dendrite penetration is easier to occur. This difference has been identified by various microscopy and spectroscopy techniques.[12,19,20,31]

In this article, I want to emphasize the electrochemical evidence related to these stability metrics. The difference in electrochemical stability can be measured by the cycling time at low current densities before the battery failure in a Li|electrolyte|Li symmetric cell. For LGPS, the cycling time is only a few hours at a current density of 0.25 mA/cm^2 before the voltage ramps up quickly to 4 V voltage (**Figure** 4a), which is a battery failure mode caused by severe electrochemical decomposition-induced ionic impedance increase at the entire primary interface between Li and LGPS. In comparison, LPSCl1.5 shows >100 h of cycling time with a voltage polarization <20 mV before a voltage sudden drop (Figure 4b), which is another failure mode caused by internal short-induced impedance drop, suggesting that the primary or secondary interface of electrolyte to Li metal or its dendrite is stable enough to allow for the complete penetration of dendrite without consuming them up at the halfway by decomposition reactions, which otherwise would show the other failure mode of voltage ramping-up instead.

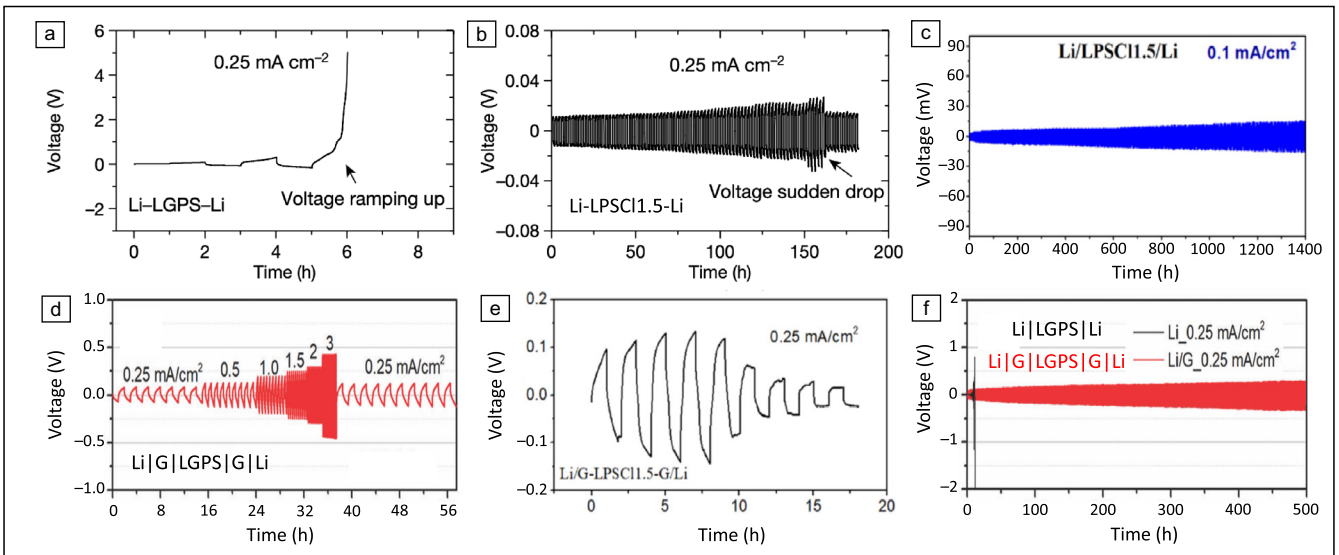

Figure 4. (a–c) Symmetric battery tests of Li|Electrolyte|Li, with the electrolyte layer being (a) LGPS[19] and (b) LPSCl1.5,[19] tested at 0.25 mA/cm^2, and (c) LPSCl1.5,[31] tested at 0.1 mA/cm^2. (d–f) Symmetric battery tests of Li|G|Electrolyte|G|Li, where G is graphite layer. (d) LGPS as electrolyte, tested at various current densities.[20] (e) LPSCl1.5[31] and (f) LGPS as electrolyte,[20] tested at 0.25 mA/cm^2. A Li|LGPS|Li battery at 0.25 mA/cm^2 is also shown in (f) for comparison. (a, b) Reprinted with permission from Reference 19. © 2021 Springer Nature. (c, e) Reprinted with permission from Reference 31. © 2022 Elsevier. (d, f) Reprinted with permission from Reference 20. © 2020 Royal Society of Chemistry.

Furthermore, at a lower current density of 0.1 mA/cm^2, more than 1400 h can be cycled for LPSCl1.5 at <15 mV polarization voltage (Figure 4c), confirming that the Li|LPSCl1.5 interface is in fact electrochemically very stable. The short circuit in Figure 4b means that for such a stable interface of little reactions, Li dendrite growth can be driven by the slightly increased current density of 0.25 mA/cm^2 to easily penetrate through the entire electrolyte layer. Overall, LGPS has a much lower electrochemical stability than LPSCl1.5 at the interface to Li metal, and hence exhibits higher hull energy G_{hull} (LGPS) > G_{hull} (LPSCl1.5) for more severe interface reactions with Li metal. On the other hand, due to the lack of reaction, Li dendrite is easier to penetrate the LPSCl1.5 layer.

However, when the electrolytes are put in another type of symmetric battery with a configuration of Li|graphite|electrolyte|graphite|Li, a different trend is observed from the symmetric battery cycling, unveiling the property of dynamic voltage stability. LGPS now shows no sign of short circuit at high current densities from 3 to 10 mA/cm^2; afterward, it can largely recover the normal cycling voltage range at a low current density of 0.25 mA/cm^2 (Figure 4d), suggesting no severe interface decomposition after experiencing the previous cycling at high current densities. In addition, LGPS now can cycle stably at 0.25 mA/cm^2 for >500 h (Figure 4f). Note that the polarization voltage cannot be directly compared between the two types of symmetric batteries with and without the graphite layer.

As mentioned in the previous section, Li metal here will mix with graphite to form the composite layer upon battery cycling, so the *in situ* formed interface between Li metal and LGPS is under a local mechanical constriction and the reduction decomposition pathway of LGPS is changed from Equation 1 to Equation 2. The result here further shows that such an interface reaction is stable enough against both failure modes of short circuit and severe decomposition, suggesting that dynamic voltage stability limits the interface decomposition reaction at an early stage, where the decomposition serves to arrest the growth of Li dendrite to prevent the short circuit.

In contrast, LPSCl1.5 gives a short circuit-induced voltage drop after only 10 h of cycling test at a low current density of 0.25 mA/cm^2 (Figure 4e), which is 10 times shorter cycling time than the previous case without graphite (Figure 4b). This means without sufficient interface contact between LPSCl1.5 and Li metal to give the local reaction strain-induced ionic passivation at the reaction front, Li dendrite can more easily penetrate the LPSCl1.5 layer. That is, LPSCl1.5 lacks sufficient dynamic stability at the anode due to an electrochemically too stable interface with Li metal. This also further confirms that it is the dynamic stability of the central LGPS layer in the multi-electrolyte-layer configuration (Figure 2a) that suppressed the Li dendrite penetration.

Therefore, these symmetric battery tests show that LGPS exhibits higher dynamic stability against lithium dendrite penetration and lower electrochemical stability against lithium-metal anode decomposition in comparison with LPSCl1.5. This fact is also consistent with the full cell test using the multi-electrolyte-layer configuration,[19] where LGPS is suitable to serve as the central layer to arrest the growth of lithium dendrite utilizing its good dynamic stability, while LPSCl1.5 is suitable to serve as the bottom layer in contact with Li|graphite anode to provide the primary interface stability using its good electrochemical stability (Figure 2a). The current density can be increased to 43 mA/cm^2 or even higher in such a battery configuration.[17]

When a series of sulfide electrolyte materials are tested for the two metrics of electrochemical and dynamic stabilities, respectively, it is found that LGPS and LPSCl1.5 represent two extreme cases of drastically different two metrics in one material (**Figure 5**a). When tuning the Cl composition to 1.0 and 0.5 in argyrodite sulfide electrolytes, the two electrochemical metrics are less different (Figure 5a), and the failure mode is mainly dominated by severe interface decomposition.[31] This explains why LPSCl1.0 can still cycle reasonably well without

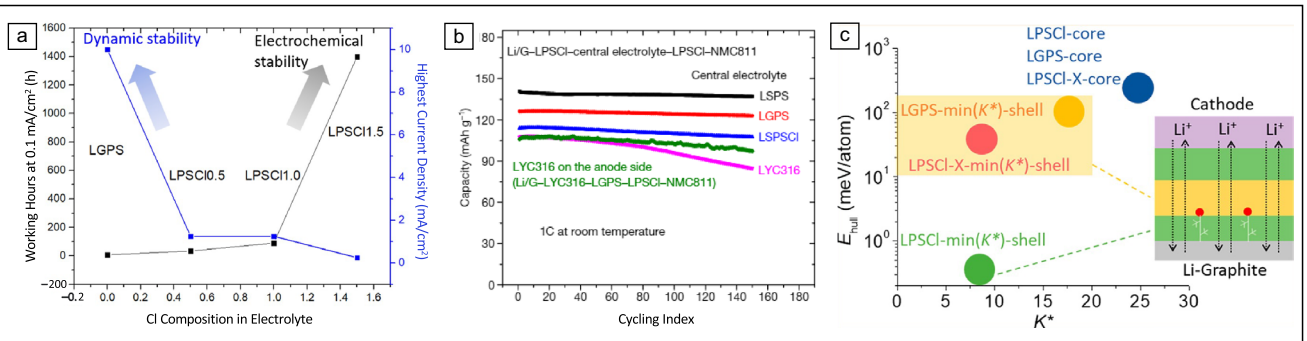

Figure 5. (a) Summary of the cycling hours at low current density (0.1–0.25 mA/cm^2) in a Li|Electrolyte|Li battery for different electrolytes of LGPS, LPSCl0.5, LPSCl1.0, LPSCl1.5 (left axis, black curve), in comparison with highest cyclable current density without battery failure in a Li|G|Electrolyte|G|Li battery (right axis, blue curve). Data points are obtained from References 19, 20, 31. (b) Cycling of different multi-electrolyte-layer configurations.[19] (c) Two-parameter space defined by interface decomposition hull energy (E_{hull}), defined as the absolute value of G_{hull}, and critical effective modulus (K^*),[17] which is a stricter criterion than K_{crit} that requires decomposition energies to be zero at any interface reaction composition (i.e., E_{hull} (x) = 0 at any x when $K_{eff} = K^*$). (b) Reprinted with permission from Reference 19. © 2021 Springer Nature. (c) Reprinted with permission from Reference 17. © 2022 American Chemical Society.

a multi-electrolyte-layer configuration when the current density is not too high.

However, when pushing to the extreme, the multi-electrolyte-layer configuration still shows the highest critical current density. This is because the configuration can decouple the two stability-metrics of dynamic and electrochemical stabilities to two different electrolyte layers that were separately optimized for an individual metric. This greatly expands the battery design flexibility. Thus, sulfide, halide, and oxide electrolytes all can be combined with each other to greatly expand battery configurations (Figure 5b). A good configuration should exhibit device level dynamic stability, following the principle discussed above to put electrochemically stable material as the bottom layer in contact with lithium metal and graphite anode, and to put dynamically stable electrolyte material as the layer above. In contrast, relying on one electrolyte to have both metrics optimized simultaneously is a constraint to the design, as the material optimization often leads to the enhancement of one metric at the expense of another.

Design dynamic voltage stability for functional interface reactions

Understanding the above fundamentals about interface reaction is important to the computational design of materials through composition control for solid-state batteries with enhanced dynamic voltage stability at various interfaces.

A metric of critical effective modulus K_{crit} was introduced, which is defined as the threshold K_{eff} at an interface reaction to make $G_{hull} = K_{crit}\epsilon V$[17,18] (Figure 1b), K_{crit} helps couple decomposition energy, reaction strain, and ionic passivation together. For a given decomposition energy G_{hull}, larger reaction strain means smaller critical modulus and larger reduction of ionic conductivity at the reaction front for the ionic passivation. Because both interface reaction energy and reaction strain can be computed *ab initio* and are composition- and phase-dependent, correlating them thus forms the foundation for the machine learning prediction of new compositions with adjustable dynamic voltage stability.

To enhance dynamic voltage stability at an interface, our goal is to adjust the chemical composition of a solid electrolyte or an electrode coating, so that the interface reaction can show reduced critical modulus K_{crit} to be more easily suppressed by local mechanical constriction at an early stage. Meanwhile, we also want to adjust the reaction hull energy G_{hull} into a certain range, because one precondition for dynamic voltage stability to function is for the reaction to happen. Thus, if G_{hull} is too low and the reaction cannot initiate sufficiently, such as LPSCl1.5 in Figure 5c (the green dot), the material is only good to serve as the bottom layer in direct contact with the Li-metal anode for good electrochemical stability at the primary interface, but it cannot serve as the central electrolyte layer to arrest the dendrite. In contrast, materials like LGPS in Figure 5c (the yellow dot) occupy a space with sufficient decomposition reaction with Li dendrite and then the reaction can be stopped quickly in a self-limiting way due to a low critical constriction modulus.

Interface reaction energy and critical modulus both can be computed *ab initio,* thus form a two-parameter space to design advanced solid electrolyte (Figure 5c). By machine learning analysis of a high-throughput *ab initio* computational database, such a design strategy guides the design of halogen-doped argyrodite electrolyte (e.g., $Li_{5.5}PS_{4.5}Cl_{1.35}I_{0.15}$) that occupies a similar region in the two-parameter space (e.g., the red dot) as LGPS, which gives >43 mA/cm^2 current density. Note that for these sulfide electrolyte materials, the core–shell microstructure[17,29] also forms an additional degree of freedom to fine-tune the property of materials, where the shell composition can be adjusted with enhanced dynamic voltage stability with the core maintaining a high ionic conductivity. The principle has also been applied to design cathode electrolyte materials with enhanced dynamic stability in an oxidative reaction[18] and cathode coatings as well,[28] and to design advanced anode materials such as Mg alloys by a new concept of constriction susceptibility derived from the dynamic stability here.[24] In addition, these self-limiting interface reactions also help glue the interface together dynamically to maintain the interface contact in a breathing battery device, unlike a propagating interface reaction or an interface without sufficient reaction that will break the interface contact upon cycling.

Summary and outlook

Understanding and utilizing interface reactions forms one important aspect to develop advanced solid-state batteries. This article emphasized the importance of the mechanical constriction effect in modulating thermodynamic and kinetic interface stabilities, giving the crucial dynamic voltage stability. Local strain energy and ionic passivation work together to stabilize the electrolyte interface reaction with electrode materials. Fully utilizing the effect shows opportunities for breakthrough solid-state battery performance beyond commercial Li-ion batteries.

Furthermore, our constrained ensemble description of dynamic voltage stability does not rely on external operational pressure, but reflects more on the intrinsic properties of materials that can be designed through composition modification. To fully lift the requirement of external pressure in practice, the proper polymer binder in the slurry casting technique and advanced assembly technique such as isotropic press at an elevated temperature to achieve and maintain low porosity during battery cycling will be important. Fortunately, it has been shown that decent cycling at a few megapascals is possible, and many approaches developed by the field at high operational pressures can be transferred toward the desired low-pressure range. To design low-pressure solid-state batteries with paradigm-shift performance, however, it will still need further nontrivial engineering development, where I hope the fundamental understanding of interface reactions reviewed here can provide some help.

Author contributions

Not applicable.

Funding

The author thanks the funding support from the US Department of Energy Vehicle Technologies Office.

Data availability

Not applicable.

Conflict of interest

On behalf of all authors, the corresponding author states that there is no conflict of interest.

References

1. C. Zhu, T. Fuchs, S.A. Weber, F.H. Richter, G. Glasser, F. Weber, H.J. Butt, J. Janek, R. Berger, *Nat. Commun.***14**, 1300 (2023)
2. Z. Ning, D.S. Jolly, G. Li, R. De Meyere, S.D. Pu, Y. Chen, J. Kasemchainan, J. Ihli, C. Gong, B. Liu, D.L.R. Melvin, A. Bonnin, O. Magdysyuk, P. Adamson, G.O. Hartley, C.W. Monroe, T.J. Marrow, P.G. Bruce, *Nat. Mater.* **20**, 1121 (2021)
3. A. Sakuda, A. Hayashi, M. Tatsumisago, *Sci. Rep.* **3**, 2261 (2013)
4. K. Hikima, M. Totani, S. Obokata, H. Muto, A. Matsuda, *ACS Appl. Energy Mater.* **5**, 2349 (2022)
5. C.E. Athanasiou, X. Liu, M.Y. Jin, E. Nimon, S. Visco, C. Lee, M. Park, J. Yun, N.P. Padture, H. Gao, B.W. Sheldon, *Cell Rep. Phys. Sci.* **3**, 100845 (2022)
6. K. Kim, D. Park, H.-G. Jung, K.Y. Chung, J.H. Shim, B.C. Wood, S. Yu, *Chem. Mater.* **33**, 3669 (2021)
7. Z. Deng, Z. Wang, I.-H. Chu, J. Luo, S.P. Ong, *J. Electrochem. Soc.* **163**, A67 (2015)
8. Y. Kato, S. Hori, T. Saito, K. Suzuki, M. Hirayama, A. Mitsui, M. Yonemura, H. Iba, R. Kanno, *Nat. Energy* **1**(4), 16030 (2016)
9. N. Kamaya, K. Homma, Y. Yamakawa, M. Hirayama, R. Kanno, M. Yonemura, T. Kamiyama, Y. Kato, S. Hama, K. Kawamoto, A. Mitsui, *Nat. Mater.* **10**, 682 (2011)
10. T. Asano, A. Sakai, S. Ouchi, M. Sakaida, A. Miyazaki, S. Hasegawa, *Adv. Mater.* **30**, 1803075 (2018)
11. X. Li, "Constrictions Induced Metastability and Kinetic Stability for Advanced Solid-State Battery Design," in *Encyclopedia of Energy Storage,* ed. by L.F. Cabeza (Elsevier, Oxford, 2022), vol. 4, p. 180
12. L. Ye, W. Fitzhugh, E. Gil-González, Y. Wang, Y. Su, H. Su, T. Qiao, L. Ma, H. Zhou, E. Hu, X. Li, *Adv. Energy Mater.* **10**(34), 2001569 (2020)
13. W. Fitzhugh, L. Ye, X. Li, *J. Mater. Chem. A Mater.* **7**, 23604 (2019)
14. Y.-G. Lee, S. Fujiki, C. Jung, N. Suzuki, N. Yashiro, R. Omoda, D.-S. Ko, T. Shiratsuchi, T. Sugimoto, S. Ryu, J.H. Ku, T. Watanabe, Y. Park, Y. Aihara, D. Im, I.T. Han, *Nat. Energy* **5**, 299 (2020)
15. J. Woo, Y.B. Song, H. Kwak, S. Jun, B.Y. Jang, J. Park, K.T. Kim, C. Park, C. Lee, K.-H. Park, H.-W. Lee, Y.S. Jung, *Adv. Energy Mater.* **13**, 2203292 (2023)
16. Y. Li, S. Song, H. Kim, K. Nomoto, H. Kim, X. Sun, S. Hori, K. Suzuki, N. Matsui, M. Hirayama, T. Mizoguchi, T. Saito, T. Kamiyama, R. Kanno, *Science* **381**(6653), 50 (2023)
17. Y. Wang, L. Ye, X. Chen, X. Li, *J. Am. Chem. Soc.* **2**, 886 (2022)
18. W. Fitzhugh, X. Chen, Y. Wang, L. Ye, X. Li, *Energy. Environ. Sci.* **14**, 4574 (2021)
19. L. Ye, X. Li, *Nature* **593**, 218 (2021)
20. Y. Su, L. Ye, W. Fitzhugh, Y. Wang, E. Gil-González, I. Kim, X. Li, *Energy Environ. Sci.* **13**, 908 (2020)
21. W. Fitzhugh, F. Wu, L. Ye, H. Su, X. Li, *Small* **15**, 1901470 (2019)
22. D.K. Singh, T. Fuchs, C. Krempaszky, P. Schweitzer, C. Lerch, F.H. Richter, J. Janek, *Matter* **6**, 1463 (2023)
23. D.H.S. Tan, Y.-T. Chen, H. Yang, W. Bao, B. Sreenarayanan, J.-M. Doux, W. Li, B. Lu, S.-Y. Ham, B. Sayahpour, J. Scharf, E.A. Wu, G. Deysher, H.E. Han, H.J. Hah, H. Jeong, J.B. Lee, Z. Chen, Y.S. Meng, *Science* **373**(6562), 1494 (2021)
24. L. Ye, Y. Lu, Y. Wang, J. Li, X. Li, *Nat. Mater.* (in press)
25. Z. Ning, G. Li, D.L.R. Melvin, Y. Chen, J. Bu, D. Spencer-Jolly, J. Liu, B. Hu, X. Gao, J. Perera, C. Gong, S.D. Pu, S. Zhang, B. Liu, G.O. Hartley, A.J. Bodey, R.I. Todd, P.S. Grant, D.E.J. Armstrong, T.J. Marrow, C.W. Monroe, P.G. Bruce, *Nature* **618**, 287 (2023)
26. W.D. Richards, L.J. Miara, Y. Wang, J.C. Kim, G. Ceder, *Chem. Mater.* **28**, 266 (2016)
27. Y. Zhu, X. He, Y. Mo, *J. Mater. Chem. A Mater.* **4**, 3253 (2016)
28. Y. Wang, L. Ye, W. Fitzhugh, X. Chen, X. Li, *Adv. Energy Mater.* **13**(41), 2302288 (2023).
29. F. Wu, W. Fitzhugh, L. Ye, J. Ning, X. Li, *Nat. Commun.* **9**, 4037 (2018)
30. H. Guo, M.R. Carbone, C. Cao, J. Qu, Y. Du, S.-M. Bak, C. Weiland, F. Wang, S. Yoo, N. Artrith, A. Urban, D. Lu, *Sci. Data* **10**, 349 (2023)
31. E. Gil-González, L. Ye, Y. Wang, Z. Shadike, Z. Xu, E. Hu, X. Li, *Energy Storage Mater.* **45**, 484 (2022)

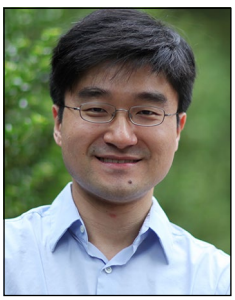

Xin Li joined the John A. Paulson School of Engineering and Applied Sciences at Harvard University in 2015, and is now an associate professor of materials science. His research group designs new energy-related materials and devices through advanced characterization, synthesis, and simulation, with the current focus on Li and Na solid-state batteries. He received his BS degree in physics from Nanjing University, China, his PhD degree in materials science and engineering from The Pennsylvania State University, and completed postdoctoral research at the California Institute of Technology and Massachusetts Institute of Technology before joining Harvard University. Li can be reached by email at lixin@seas.harvard.edu.